The Astrophysical Journal, 975:6 (13pp), 2024 November 1 https://doi.org/10.3847/1538-4357/ad702e

Ultraviolet Flux and Spectral Variability Study of Blazars Observed with UVIT/AstroSat

M. Reshma[1], Aditi Agarwal[2], C. S. Stalin[3], Prajwel Joseph[1,3], Akanksha Dagore[3], Amit Kumar Mandal[4], Ashish Devaraj[1], and S. B. Gudennavar[1]
[1] Department of Physics and Electronics, CHRIST University, Bangalore 560 029, India; shivappa.b.gudennavar@christuniversity.in
[2] Centre for Cosmology and Science Popularization, SGT University, Gurugram 122 505, India
[3] Indian Institute of Astrophysics, Block II, Koramangala, Bangalore 560 034, India; stalin@iiap.res.in
[4] Department of Physics & Astronomy, Seoul National University, Seoul 08826, Republic of Korea
Received 2024 July 22; revised 2024 August 7; accepted 2024 August 7; published 2024 October 21

Abstract

Blazars, the peculiar class of active galactic nuclei, are known to show flux variations across the accessible electromagnetic spectrum. Though they have been studied extensively for their flux variability characteristics across wavelengths, information on their ultraviolet (UV) flux variations on timescales of hours is very limited. Here, we present the first UV flux variability study on intraday timescales of a sample of ten blazars comprising two flat-spectrum radio quasars (FSRQs) and eight BL Lacertae objects (BL Lacs). These objects, spanning a redshift (z) range of $0.034 \leqslant z \leqslant 1.003$, were observed in the far-UV (1300−1800 Å) and near-UV (2000−3000 Å) wavebands using the ultraviolet imaging telescope on board AstroSat. UV flux variations on timescales of hours were detected in nine sources out of the observed ten blazars. The spectral variability analysis showed a bluer-when-brighter trend with no difference in the UV spectral variability behavior between the studied sample of FSRQs and BL Lacs. The observed UV flux and spectral variability in our sample of both FSRQs and BL Lacs revealed that the observed UV emission in them is dominated by jet synchrotron process.

Unified Astronomy Thesaurus concepts: Active galactic nuclei (16); Blazars (164); BL Lacertae objects (158); Flat-spectrum radio quasars (2163); Ultraviolet photometry (1740)

Materials only available in the online version of record: machine-readable table

1. Introduction

Active galactic nuclei (AGN), the high luminosity ($10^{11}-10^{14}\,L_{\odot}$) sources in the Universe, are thought to be powered by the accretion of matter onto supermassive black holes (SMBHs: $10^{6}-10^{10}\,M_{\odot}$) situated at the center of galaxies (D. Lynden-Bell 1969; M. J. Rees 1984). About 10% of AGN emit copiously in the radio band, display relativistic jets, and emit over a wide range of the electromagnetic spectrum from low-energy radio waves to high-energy (TeV) γ-rays. A minority of these objects having their relativistic jets oriented close to the line of sight to the observer ($\leqslant 10^{\circ}$) are called blazars (R. Antonucci 1993; C. M. Urry & P. Padovani 1995). The broadband spectral energy distribution (SED) of blazars is dominated by the beamed emission from relativistic particles in their jet (R. D. Blandford & M. J. Rees 1978; C. M. Urry & P. Padovani 1995).

Blazars are divided into flat-spectrum radio quasars (FSRQs) and BL Lacertae objects (BL Lacs), with FSRQs having broad emission lines with equivalent width above 5 Å and BL Lacs having either featureless spectra or spectra with weak emission lines with equivalent width below 5 Å. A more physical distinction between FSRQs and BL Lacs is based on the luminosity of the broad-line region ($L_{\rm BLR}$) relative to the Eddington luminosity ($L_{\rm Edd}$) with the dividing line set at $L_{\rm BLR}/L_{\rm Edd} \sim 5 \times 10^{-4}$ (G. Ghisellini et al. 2011). The broadband SED of blazars has a two-hump structure. The low-energy hump peaking in the optical/infrared/soft X-ray region is attributed to synchrotron emission process (C. M. Urry & R. F. Mushotzky 1982), and the high-energy hump peaking in the X-ray/MeV region is attributed to inverse Compton scattering process (A. A. Abdo et al. 2010). Based on the position of the synchrotron peak ($\nu_{\rm peak}$) in their broadband SED, blazars are further divided into low-synchrotron-peaked (LSP; $\nu_{\rm peak} < 10^{14}$ Hz), intermediate-synchrotron-peaked (10^{14} Hz $< \nu_{\rm peak} < 10^{15}$ Hz), and high-synchrotron-peaked (HSP; $\nu_{\rm peak} > 10^{15}$ Hz) blazars (A. A. Abdo et al. 2010).

In addition, an important characteristic of blazars is that they show flux variations over the entire accessible electromagnetic spectrum on a range of timescales from minutes to hours (S. J. Wagner & A. Witzel 1995; M.-H. Ulrich et al. 1997; J. R. Webb 2021). Such flux variations can serve as an efficient tool to understand the nature of the central regions and the jets of blazars. The flux variations are also known to be correlated across wavelengths, supporting the argument that the low-energy and the high-energy emissions arise from the same population of relativistic electrons in the jet via synchrotron and inverse Compton processes, respectively (M.-H. Ulrich et al. 1997). However, recent observations point to varied correlations between low-energy optical and high-energy γ-ray observations, indicating the lack of our understanding on the flux variability characteristics of blazars (B. Rajput et al. 2020, 2021). In addition to flux variations, blazars also show large optical and infrared polarization (J. R. P. Angel & H. S. Stockman 1980) and optical polarization variations (S. Rakshit et al. 2017; A. Pandey et al. 2022; B. Rajput et al. 2022). Though blazars have been studied for variability across multiple wavelengths, on a range of timescales, their ultraviolet (UV) variability characteristics are not explored much, with only sparse reports available in the literature (R. Edelson 1992). Understanding the UV flux variations in blazars is important as the UV emission in the

Table 1
Details of the Sources Studied in This Work

Name	R.A. (hh:mm:ss)	Decl. (dd:mm:ss)	Type/Subtype	z
PKS 0208−512	02:10:46.20	−51:01:01.89	FS/LSP	1.003
1ES 0229+200	02:32:48.62	+20:17:17.48	BL/HSP	0.140
OJ 287	08:54:48.88	+20:06:30.64	BL/LSP	0.306
1ES 1101−232	11:03:37.61	−23:29:31.20	BL/HSP	0.186
1ES 1218+304	12:21:21.94	+30:10:37.16	BL/HSP	0.182
H 1426+428	14:28:32.61	+42:40:21.05	BL/HSP	0.129
PKS 1510−089	15:12:50.53	−09:05:59.83	FS/LSP	0.360
Mrk 501	16:53:52.22	+39:45:36.61	BL/HSP	0.034
PKS 2155−304	21:58:52.07	−30:13:32.12	BL/HSP	0.116
1ES 2344+514	23:47:04.84	+51:42:17.88	BL/HSP	0.044

Note. Here, R.A., Decl., and z are the R.A., Decl., and redshift of the sources, respectively (M.-P. Veron-Cetty & P. Veron 2010). FS refers to FSRQ and BL refers to BL Lac; LSP and HSP refer to LSP and HSP blazars.

broadband SED of blazars is usually dominated by synchrotron emission from relativistic jet electrons (A. A. Abdo et al. 2011; V. S. Paliya et al. 2015). However, in the faint state, the signature of the prominent accretion-disk emission in the optical-UV region is evident in the broadband SED of the FSRQ category of blazars (G. Bonnoli et al. 2011; V. S. Paliya et al. 2016, 2017). Some recent studies do exist that focus on UV variability of AGN sources, mainly from Galaxy Evolution Explorer (GALEX) and International Ultraviolet Explorer (IUE) observations (B. Y. Welsh et al. 2011; N. Sukanya et al. 2018). However, these studies are focused on flux variations in nonblazar-type AGN on longer timescales.

In this work, UV variability characteristics of blazars on hour-like timescales are studied using the data from the UV imaging telescope (UVIT; S. N. Tandon et al. 2017, 2020) on board AstroSat. This is the first study where the temporal and spectral properties of ten blazars in UV on intraday timescales are investigated. The paper is structured as follows: in Section 2, observations and data reduction procedures are described. In Section 3, the analysis technique used to study the temporal and spectral variability properties of the sample of sources is detailed, while the notes on individual sources and the results are detailed in Section 4. Finally, discussion and conclusions are presented in Section 5.

2. Observations and Data Reduction

The sample of sources used for this study was selected from the archives of observations carried out by UVIT (S. N. Tandon et al. 2017, 2020), one of the payloads on board India's multiwavelength astronomical observatory, AstroSat (P. C. Agrawal 2017), launched by the Indian Space Research Organization on 2015 September 28. UVIT, with a field of view of ∼28′ diameter, observes simultaneously in two channels, namely, the far-UV (FUV: 1300 −1800 Å) and the near-UV (NUV: 2000−3000 Å) using a set of filters. It also has a visual channel (3200−5500 Å), which is used for tracking the aspects of the telescope and is used in the processing of the data while generating science-ready images in the FUV and NUV channels. The details of the sources studied in this work are given in Table 1. The log of observations of the sources used in this work is given in Table 2, and the details of the filters used are given in Table 3.

The science-ready images of the observations available at the Indian Space Science Data Center (ISSDC)[5] are used in this work. The images were made available to ISSDC by the Payload Operations Center (POC) at the Indian Institute of Astrophysics, Bangalore. At the POC, the images were reduced using the UVIT L2 pipeline version 6.3 (S. K. Ghosh et al. 2021, 2022). The pipeline creates science-ready images by correcting the raw data for spacecraft drift, flat-field, and geometric distortion. The observed fields of the sources are given in Figure 1. The aperture photometry for one of the target sources, 1ES 1218+304, for a radius of 12 subpixels, was carried out using the Photutils Python package (L. Bradley et al. 2023). The background was removed using the local background subtraction method, where a circular annular region with an inner radius of 150 subpixels and an outer radius of 200 subpixels were used. The background-subtracted source light curve obtained using Photutils was compared with the light curve generated using the Curvit Python package (P. Joseph et al. 2021; Figure 2). From Figure 2, it is evident that both light curves are very well matched. The mean of the differences between the two light curves (bottom panel of Figure 2) was found to be 0.016 ± 0.003 mag. This is due to the systematically fainter magnitudes from Photutils as the derived magnitudes were not corrected for saturation effects. The advantage of Curvit over Photutils is that Curvit works on the calibrated events list, while Photutils works on the images. Therefore, for the rest of the sample sources, the Curvit package (P. Joseph et al. 2021) was used to generate the light curves. In each source, the individual orbit-wise event lists were combined using Curvit package, and the combined events list was used for generating the light curves. In addition to background subtraction, the light curves were also subjected to aperture and saturation correction. The brightness of the blazars derived over a circular aperture of 12 subpixel radii using Curvit was then converted to the total brightness using Table 11 of S. N. Tandon et al. (2020). The brightness of all the blazars thus obtained is given in the Appendix.

3. Analysis

3.1. Flux Variability

The intrinsic amplitude of flux variability, which is basically the observed variance of the light curve after the removal of the measurement errors, was calculated to characterize variability. The intrinsic amplitude of flux variability, σ_m (mag), is defined as (Y. L. Ai et al. 2010)

$$\sigma_m = \sqrt{(\Sigma^2 - \epsilon^2)}. \quad (1)$$

Here, Σ^2 is the observed variance and is given by

$$\Sigma = \sqrt{\frac{1}{N-1}\sum_{i=1}^{N}(m_i - \langle m \rangle)^2}, \quad (2)$$

where N is the number of orbits and $\langle m \rangle$ is the weighted mean of the m_i measurements with errors ϵ_i. ϵ is the contribution of measurement errors to the variance and is defined as

$$\epsilon^2 = \frac{1}{N}\sum_{i=1}^{N}\epsilon_i^2. \quad (3)$$

A source was considered variable if $\Sigma^2 > \epsilon^2$, else, $\sigma_m = 0$.

[5] https://www.issdc.gov.in/astro.html

Table 2
Log of Observations

Name	Date of Observation (dd-mm-yyyy)	OBSID	Filter	MJD Start	MJD End	Net Exposure Time (s)
PKS 0208−512	30-10-2016	A02-114T01-9000000764	F148W	57690.991247	57691.386868	1337
			F169M	57691.588337	57691.731484	1710
			N219M	57690.991175	57691.524076	2236
			N279N	57691.588288	57691.863146	2119
	25-12-2019	T03-170T01-9000003388	F148W	58841.831743	58841.833213	119
			F154W	58841.904312	58841.905736	116
			F169M	58841.976881	58842.311886	1223
			F172M	58842.508345	58842.654596	1037
1ES 0229+200	01-10-2017	A04-130T01-9000001572	F154W	58027.768812	58027.926301	4922
			N245M	58027.768763	58027.926351	4951
	09-12-2017	A04-130T01-9000001762	F154W	58096.737591	58096.944207	4970
			N245M	58096.737542	58096.944257	5005
	22-12-2017	A04-130T01-9000001792	F154W	58108.834869	58109.180995	3962
			N245M	58108.834820	58109.109934	5046
	08-01-2018	A04-130T01-9000001822	F154W	58126.562901	58126.779650	4974
			N245M	58126.562852	58126.779700	5006
OJ 287	10-04-2017	T01-163T01-9000001152	F169M	57852.921707	57853.686358	8422
			N245M	57852.921656	57853.415465	4501
			N263M	57853.417144	57853.686437	3649
	18-04-2018	A04-199T01-9000002040	F169M	58225.694593	58227.596754	25365
			F172M	58223.458444	58225.692828	28154
	18-05-2020	T03-206T01-9000003672	F148W	58984.390970	58984.732999	3636
			F154W	58984.734732	58985.407435	4855
			F172M	58986.764797	58987.710244	6497
			F148Wa	58985.409168	58986.561064	3782
1ES 1101−232	30-12-2016	G06-086T02-9000000936	F154W	57750.400520	57752.501664	33497
			N263M	57750.400471	57752.501714	33926
1ES 1218+304	21-05-2016	G05-211T01-9000000464	F148W	57528.302435	57529.431526	13881
			N245M	57528.302745	57529.431577	13847
H 1426+428	05-03-2018	A04-094T01-9000001942	F148W	58181.865544	58182.463086	6836
			F154W	58181.577434	58181.863807	7940
			N242W	58181.577385	58181.781955	5110
			N245M	58181.783577	58182.463086	9772
PKS 1510−089	30-03-2016	T01-106T01-9000000404	F172M	57476.398455	57478.031161	26663
			N219M	57476.398407	57478.031211	26866
	16-03-2018	A04-101T01-9000001984	F172M	58192.878269	58193.695960	13270
			N219M	58192.878220	58193.696009	13349
	15-06-2018	A04-101T01-9000002170	F172M	58284.086589	58284.771371	12085
Mrk 501	15-08-2016	G05-218T05-9000000602	F154W	57615.260263	57615.946790	12154
			N219M	57615.255611	57615.946840	12639
	28-03-2020	A07-145T01-9000003594	F148W	58935.087363	58937.726873	25484
PKS 2155−304	21-05-2018	A04-130T03-9000002108	F154W	58259.329918	58259.544023	2788
	24-06-2018	A04-130T03-9000002186	F154W	58293.495067	58293.579373	2842
	16-09-2019	A05-117T01-9000003166	F154W	58742.571362	58742.777812	4117
1ES 2344+514	06-06-2017	A03-033T01-9000001276	F172M	57910.717527	57910.863068	2195
			N245M	57910.717477	57910.860639	2015
	09-07-2017	A03-033T01-9000001368	F172M	57943.391924	57943.546931	3586
			N245M	57943.391873	57943.549083	3718
	07-08-2017	A03-033T01-9000001438	F172M	57972.282651	57972.430529	3886
			N245M	57972.282601	57972.428121	3705
	07-09-2017	A03-033T01-9000001524	F172M	58003.815110	58003.972611	3977
			N245M	58003.815060	58003.972663	4000
	22-11-2017	A04-049T01-9000001710	N245M	58078.933083	58079.201251	1897
	07-12-2017	A04-049T01-9000001754	F172M	58094.972718	58095.243561	1392
			N245M	58094.972670	58095.243611	1409
	12-09-2018	T02-104T01-9000002356	F172M	58372.864037	58373.064969	3439

Note. Here, name of the source, date of observation (dd-mm-yyyy), observational ID (OBSID), filters used in the observations, start and end time of the observations in modified Julian date (MJD), and the net exposure time in seconds are given in Columns (1), (2), (3), (4), (5), (6), and (7), respectively.

3.2. Spectral Variability

In order to study the various spectral trends found in blazars, different color-index combinations were obtained and plotted against the magnitude, popularly known as the color–magnitude diagram (CMD). In general, in the optical band, most BL Lacs exhibit a bluer-when-brighter (BWB) trend (F. Vagnetti et al. 2003; H.-Z. Li et al. 2024), while FSRQs

Table 3
Details of FUV and NUV Filters of UVIT Used in This Work

Filter	λ_{mean} (Å)	$\Delta\lambda$ (Å)	Zero Point (mag)
F148W	1481	500	18.097 ± 0.010
F148Wa	1485	500	18.097 ± 0.010
F154W	1541	380	17.771 ± 0.010
F169M	1608	290	17.410 ± 0.010
F172M	1717	125	16.274 ± 0.020
N242W	2418	785	19.763 ± 0.002
N219M	2196	270	16.654 ± 0.020
N245M	2447	280	18.452 ± 0.005
N263M	2632	275	18.146 ± 0.010
N279N	2792	90	16.416 ± 0.010

Note. Here, λ_{mean} is the mean wavelength, and $\Delta\lambda$ is the bandwidth (S. N. Tandon et al. 2020).

display a redder-when-brighter (RWB) trend (M. Gu et al. 2006; V. Negi et al. 2022). Color variations on hour timescales for five sources having more than four simultaneous FUV and NUV photometric observations were studied. To study the color trends quantitatively, the CMDs for all combinations were fitted with an unweighted linear least-squares fit of the form color index (CI) $= m \times M + c$, where M is the magnitude, and m and c are the slope and intercept, respectively. A positive value of the slope indicates a BWB trend, while a negative value hints toward the presence of an RWB trend. For the trend to be significant at the 99% significance level, the correlation coefficient (R) should be more than 0.5 (R. Prince et al. 2021). In addition to the unweighted least-squares fit to the points on the CMD, a weighted linear least-squares fit was also carried out by considering the errors in both the colors and the magnitudes. For this, a Bayesian linear regression with the LINMIX _ ERR method (B. C. Kelly 2007) was used. This method is effective in handling errors in both the color and magnitude measurements as well as correlations between the errors. In addition to LINMIX _ ERR, the Bivariate Correlated Errors and Intrinsic Scatter (BCES; M. G. Akritas & M. A. Bershady 1996) was also used, and the results are consistent with each other. For all the further discussions on spectral variability, the results from the Bayesian analysis are used.

4. Results

4.1. Flux Variability

All ten blazar fields used in this work are less crowded. As the goal of the present study is to characterize the UV variability of blazars on hour-like timescales, aperture photometry was carried out following the procedures outlined in Section 2. Of all the sources analyzed in this work, nine sources were found to show flux variations, except that of Mrk 501, which was found to be nonvariable. The results of the variability analysis for sources showing variability are given in Table 4, and the light curves generated for all the sample sources are given in Figures 3 and 4. Further, details of the flux variability of each of the sources are given in Section 4.3.

4.2. Spectral Variability

Flux variations in blazars are accompanied by spectral variations. The color changes in blazars on diverse timescales directly related to the spectrum of the blazar are well studied by many authors in optical bands (M. Villata et al. 2004; C. S. Stalin et al. 2009; E. Bonning et al. 2012; G. Bhatta & J. Webb 2018; H. Gaur et al. 2019; A. Agarwal 2023), but genuine color behavior at different timescales is still one of the most puzzling issues in blazar physics. Moreover, color changes on hourly timescales in the UV bands are rarely studied in blazars though a few studies exist for Seyfert-type AGN (K. Chand et al. 2022). This is the first search for dominant color trends in blazars on the intraday timescale in the UV regime. A better understanding of dominant emission mechanisms in the source can be understood through the studies on spectral variations. The UV spectral variations can be contributed by both the accretion disk and the Doppler-boosted relativistic jets. In order to understand this, CMDs were generated for the sources. For this, only the five sources that are variable and also have more than four simultaneous NUV and FUV measurements were considered. The CMDs were then analyzed following the methodology described in Section 3.2. The fits to the CMDs of the sources are given in Figure 5, and the results of the fit are given in Tables 5 and 6. A BWB trend was observed for all the sources analyzed for spectral variability. Studies in the literature (M. Villata et al. 2002; C. M. Raiteri et al. 2017) suggest that a BWB trend in blazars is due to intrinsic energetic processes in the jet.

4.3. Notes on Individual Sources

4.3.1. PKS 0208−512

PKS 0208−512 is an FSRQ of LSP type at a redshift of $z = 1.003$ (S. E. Healey et al. 2008). It has been detected by EGRET on board the Compton Gamma Ray Observatory (R. C. Hartman et al. 1999) and Fermi Gamma-ray Space Telescope (S. Abdollahi et al. 2020). It has been studied for optical and infrared flux variations on a day-like timescale (E. Bonning et al. 2012). Between 2008 August and 2011 September, the source underwent three optical and infrared bursts from monitoring observation on day-like timescales. Of the three optical infrared outbursts, only two outbursts and flares at GeV energies were observed. An RWB spectral variation was noticed in the optical and near-infrared bands (R. Chatterjee et al. 2013). It was found to show intranight optical variability (G. E. Romero et al. 2002). Variations in the UV band are reported for the first time.

4.3.2. 1ES 0229+200

1ES 0229+200 is a very-high-energy γ-ray source (F. Aharonian et al. 2007a) and also detected in the GeV energy range by the Fermi Gamma-ray Space Telescope (M. Ackermann et al. 2015). It was found to show optical flux variations within a night (R. Bachev et al. 2012) and on day-like timescales (A. Pandey et al. 2020) and very high energy (VHE) variations on month-like timescales (G. Cologna et al. 2015). It was also studied for X-ray flux variations in the 3−79 keV band using observations from NuSTAR (A. Pandey et al. 2017). It has not been studied for UV variations before. It was found to be variable on all the four epochs in which it was observed.

4.3.3. OJ 287

OJ287, believed to host a supermassive binary black hole (A. Sillanpaa et al. 1988), has been extensively studied for flux

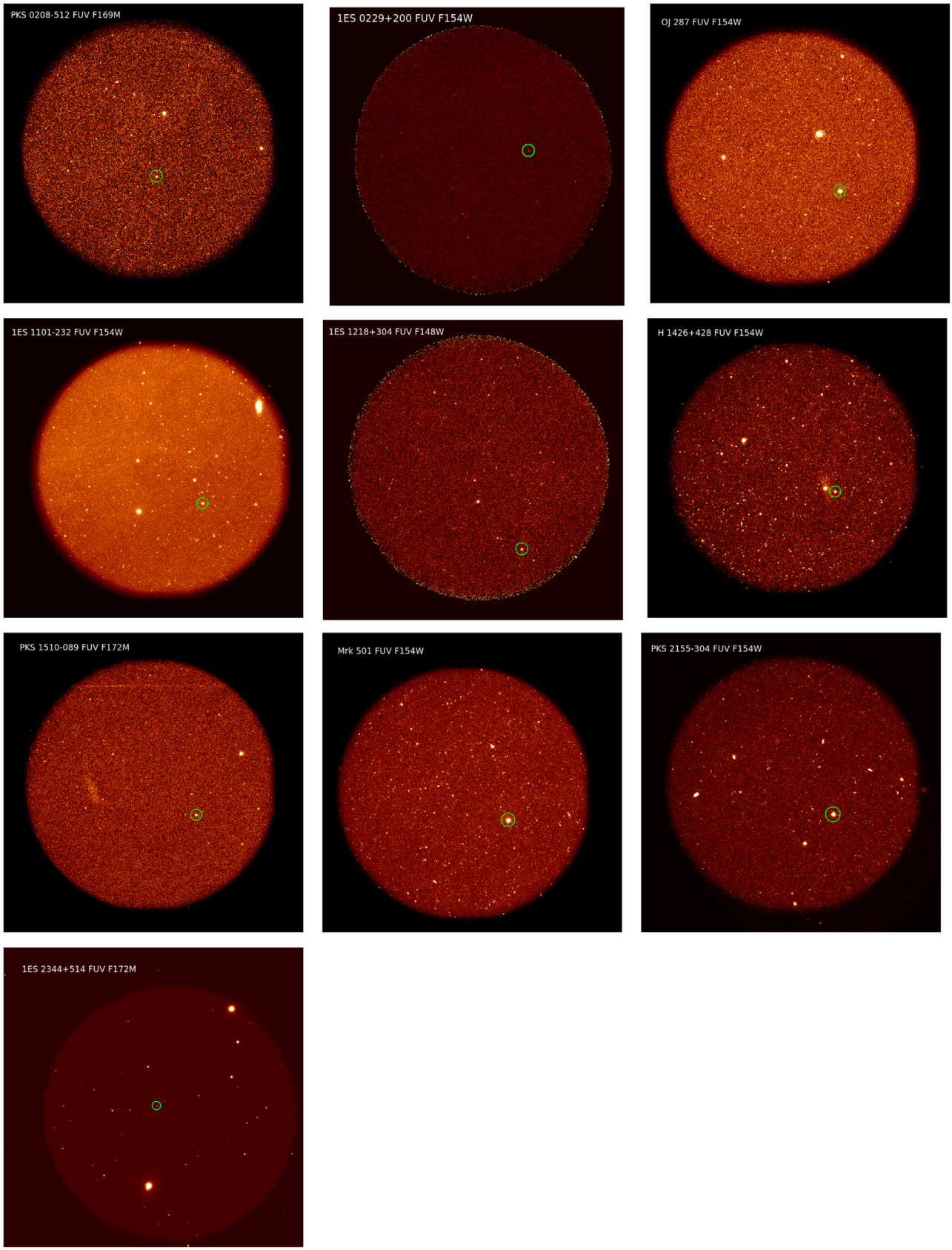

Figure 1. The observed FUV field images of the ten blazar sources. The target sources are shown in green circles. The source name and the corresponding filter name are given in each field image. Each image has a field of view of $\sim 28'$ diameter.

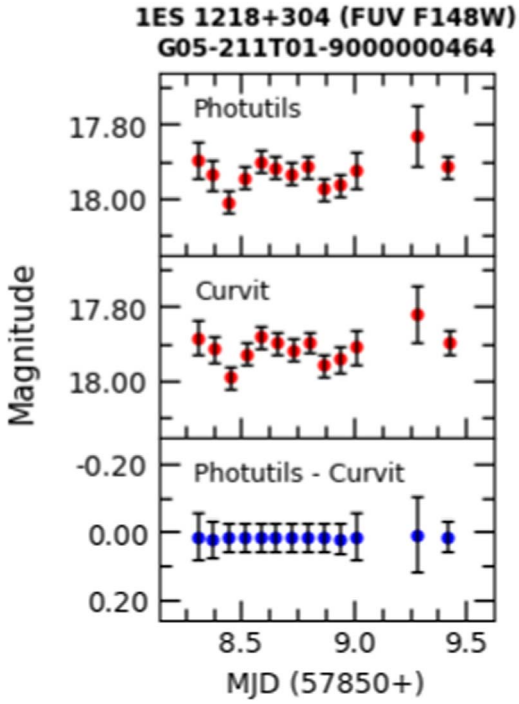

Figure 2. Comparison plot of FUV light curve for the source 1ES 1218+304 in F148W filter with top panel denoting Photutils light curve, middle panel denoting Curvit light curve, and bottom panel denoting the difference between Photutils and Curvit light curves.

variations across wavelengths on a range of timescales, including UV (R. Bachev et al. 2012; S. Huang et al. 2022), optical (S. L. O'Dell et al. 1978), and GeV γ-rays (I. Agudo et al. 2011). In addition to flux variations, the source has also been studied for optical polarization variation (S. Rakshit et al. 2017). This source was observed for three epochs simultaneously in both FUV and NUV. The source was found to show variations on all three epochs. In addition to flux variations, the source was also found to show spectral variations in one of the epochs with a BWB trend.

4.3.4. 1ES 1101−232

1ES 1101−232 is a very-high-energy BL Lac (F. Aharonian et al. 2007b). It was found to show variations in the 3−79 keV band in X-rays (A. Pandey et al. 2018), optical flux (G. E. Romero et al. 2002), and polarization microvariability. This source has no previous record on its UV flux variations. This source was observed by UVIT on 2016 December 30, with two different filters (F154W and N263M). The source was found to show flux variations on an hour-like timescale in both FUV and NUV bands. In addition to flux variability, the source was also found to show spectral variability with a BWB pattern.

4.3.5. 1ES 1218+304

1ES 1218+304 is an HSP blazar at a redshift $z = 0.182$ (J. Otero-Santos et al. 2022). It is also detected in GeV γ-rays by Fermi (P. L. Nolan et al. 2012) and in very-high-energy γ-rays from MAGIC (J. Albert et al. 2006) and from VERITAS (V. A. Acciari et al. 2009) observations. It has been studied for optical flux variations both for the long term (V. Negi et al. 2022) and within a night (G. A. Gopal-Krishna et al. 2011). It is highly polarized in the optical with a polarization degree of 6.83% ± 0.70% (B. T. Jannuzi et al. 1994). It has been found to be variable in the X-ray band in the 0.3−10 keV energy range from XMM-Newton observations (P. U. Devanand et al. 2022), in the hard X-ray band from NuSTAR observations (A. Pandey et al. 2018), and in the high-energy γ-ray band from VERITAS (V. A. Acciari et al. 2010). From Swift/UVOT, observations 1ES 1218+304 was found to show long-term variations in UV (K. E. Moo et al. 2022). However, it has not been studied for UV variations on hour-like timescales before. The source was observed on one epoch. On this epoch, the source was found to show flux variations as well as a BWB spectral variability.

Table 4
Results of Variability Analysis for Sources Showing Variability

Name	Date (dd-mm-yyyy)	Filter	N	σ_m (mag)
PKS 0208−512	30-10-2016	F148W	4	0.06
1ES 0229+200	01-10-2017	N245M	3	0.03
	09-12-2017	F154W	4	0.12
	08-01-2018	F154W	4	0.04
		N245M	4	0.05
OJ 287	10-04-2017	F169M	11	0.03
		N245M	7	0.01
	18-04-2018	F169M	24	0.03
	18-05-2020	F148W	6	0.01
		F154W	8	0.04
		F172M	10	0.04
		F148Wa	6	0.03
1ES 1101−232	30-12-2016	F154W	32	0.04
		N263M	32	0.03
1ES 1218+304	21-05-2016	F148W	13	0.01
H 1426+428	05-03-2018	F148W	8	0.03
		F154W	5	0.02
		N242W	4	0.03
PKS 1510−089	16-03-2018	F172M	11	0.02
		N219M	11	0.12
PKS 2155−304	21-05-2018	F154W	4	0.02
	16-09-2019	F154W	3	0.02
1ES 2344+514	06-06-2017	F172M	3	0.98
	09-07-2017	F172M	3	0.06
		N245M	3	0.03
	07-09-2017	F172M	3	0.02
	07-12-2017	F172M	2	0.24

Note. Here, N is the number of orbits, and σ_m is the amplitude of flux variability in magnitude.

4.3.6. H 1426+428

H 1426+428 is an extreme HSP blazar (L. Costamante et al. 2001) and was detected in TeV γ-rays from observations with the Whipple telescope (D. Horan et al. 2002) and from HEGRA observations (F. Aharonian et al. 2002). In the radio band, it has a compact core surrounded by a halo (M. Giroletti et al. 2004). From Very Long Baseline Array observations at 8 GHz, B. G. Piner et al. (2008) found the source to have a parsec-scale radio structure consisting of a core and a single jet component. It was observed to show optical flux variations within a night (G. A. Gopal-Krishna et al. 2011). It was found to show long-term flux and color variations in the optical (H. Gaur et al. 2012b; V. Negi et al. 2022) as well as flux variation in X-rays (P. U. Devanand et al. 2022). It is polarized in the optical and also shows polarization variations (T. Hovatta et al. 2016). This source has been studied for UV flux variations for the first time.

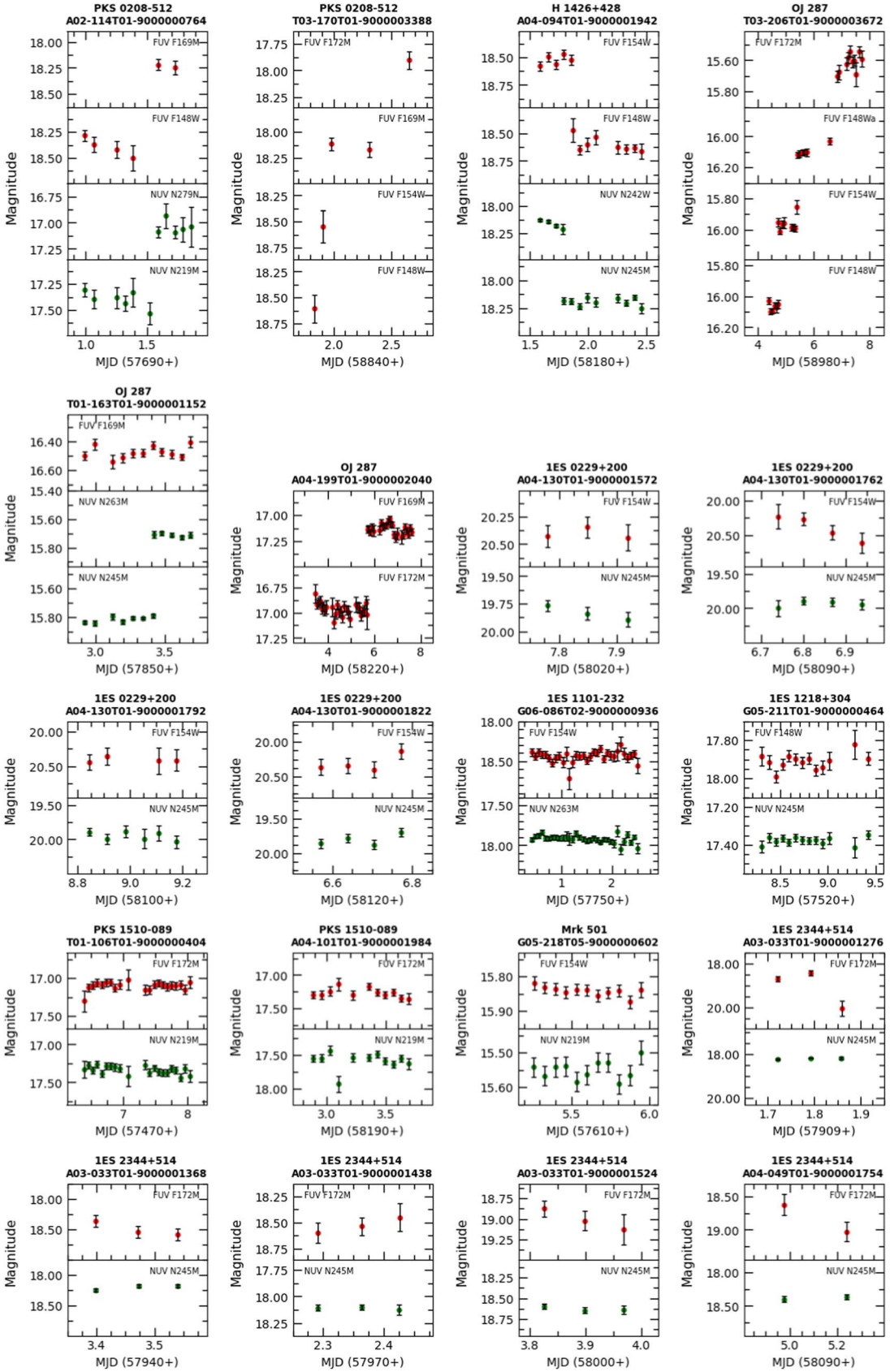

Figure 3. FUV and NUV light curves (represented by red and green circles, respectively) of sources. The observation ID and source name are labeled in each plot. The name of the filters used for the light curves is given in each panel.

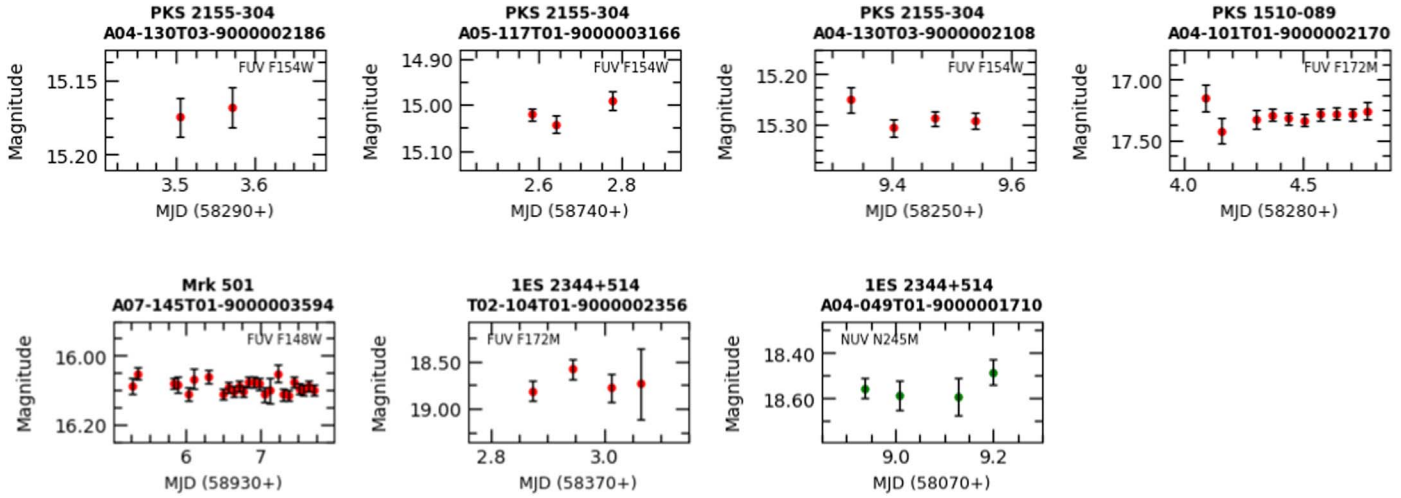

Figure 4. FUV and NUV light curves of sources. Here, red dots denote FUV light curves, and green dots denote NUV light curves. The respective source name and observation ID are mentioned on top of each plot. Also, the names of the filters used for the light curves are given in each panel.

The source was found to show both flux and spectral variations (BWB trend) on the single epoch in which it was observed.

4.3.7. PKS 1510−089

PKS 1510−089 is an FSRQ at $z = 0.360$ (D. J. Thompson et al. 1990) and is powered by a black hole of mass $5.7^{+0.62}_{0.58} \times 10^7\ M_\odot$ (S. Rakshit 2020). It is known to emit high-energy γ-rays in GeV band and also in TeV from HESS (H. E. S. S. Collaboration et al. 2013) and MAGIC (MAGIC Collaboration et al. 2018). Quasiperiodic oscillation (QPO) was detected in the GeV light curve of the source (A. Roy et al. 2022). PKS 1510−089 has been studied for correlation between flux variations between different wavelengths. The flux variations in the γ-ray and optical/IR bands were found to precede the variations in the radio band (Q. Yuan et al. 2023). While V. Ramakrishnan et al. (2016) found the long-term optical and γ-ray flux variations to be correlated with zero lag, B. Rajput et al. (2020) found complex flux variability behavior between optical and γ-ray bands. In the broadband SED, optical/UV emission was found to be dominated by emission from the accretion disk (A. Barnacka et al. 2014). It was known to show short-timescale flux variations in the optical (G. E. Romero et al. 1999, 2002; G. A. Gopal-Krishna et al. 2011) and γ-rays (S. Saito et al. 2013). It is polarized in the optical and also shows polarization variations (I. Andruchow et al. 2005). From observations carried out with IUE, the source was found to show variability in the UV continuum (P. T. Obrien et al. 1988). This source has not been studied before for short-term variations in the UV. This source was detected in three epochs. It was found to show flux and spectral variability in one of the epochs.

4.3.8. Mrk 501

Mrk 501 ($z = 0.034$) is a strong X-ray and TeV γ-ray source (E. Pian et al. 1998; A. Djannati-Atai et al. 1999) with a black hole of mass $10^{8.93\pm0.21}\ M_\odot$ (R. Falomo et al. 2002). In the radio band, at the parsec scale, the source is known to have a relativistically boosted one-sided jet (P. G. Edwards & B. G. Piner 2002). It is known to be variable in X-rays and TeV γ-rays (M. Gliozzi et al. 2006). In the optical, rapid variations on the timescale of minutes have been observed (W. Zeng et al. 2019). In addition to flux variations, optical color variations have also been observed. This source was observed for two epochs so that their UV-variability nature on hour-like timescales could be studied. On both epochs, it was found that the source does not show any variability.

4.3.9. PKS 2155−304

PKS 2155−304 is an HSP blazar situated at $z = 0.116$ (R. Falomo et al. 1993) and has been extensively studied across wavelengths. It is variable in the optical (H. Gaur et al. 2010; G. E. Romero et al. 1999), X-rays (Z. Zhang et al. 2021), γ-rays (F. M. Rieger & F. Volpe 2010), UV from observations with the IUE (C. M. Urry et al. 1993), and in the extreme UV from the Extreme Ultraviolet Explorer observations (H. L. Marshall et al. 2001). QPO has been detected in the optical (A. Sandrinelli et al. 2014), X-ray (P. Lachowicz et al. 2009), and GeV γ-rays (H. X. Ren et al. 2023). It is polarized in the optical and also shows polarization variations (N. W. Peceur et al. 2020). This source was observed for three epochs in the FUV band, and on all the occasions, it was found to be variable.

4.3.10. 1ES 2344+514

The source 1ES 2344+514 at a redshift of $z = 0.044$ (E. S. Perlman et al. 1996) is an X-ray source detected in the Einstein Slew Survey (M. Elvis et al. 1992) and is also a VHE γ-ray emitter (M. Catanese et al. 1998). It is also detected by VERITAS (V. A. Acciari et al. 2011) and MAGIC (MAGIC Collaboration et al. 2020). It was found to have short-timescale variation in X-rays (P. Giommi et al. 2000) and optical (A. Pandey et al. 2020). In the optical, it was also found to show variations on day-like timescales (X. Dai et al. 2001; H. Gaur et al. 2012a; Z.-Y. Cai et al. 2022). It is also variable in γ-rays (J. Grube 2008). On long timescales, it is found to be variable in UV based on observations with the Swift/UVOT acquired over a period of 3 yr from 2019 to 2021 (T. Abe et al. 2024). This source has been observed for seven epochs so that its UV-variability nature on hour-like timescales could be studied. The source was found to show flux variability on four epochs.

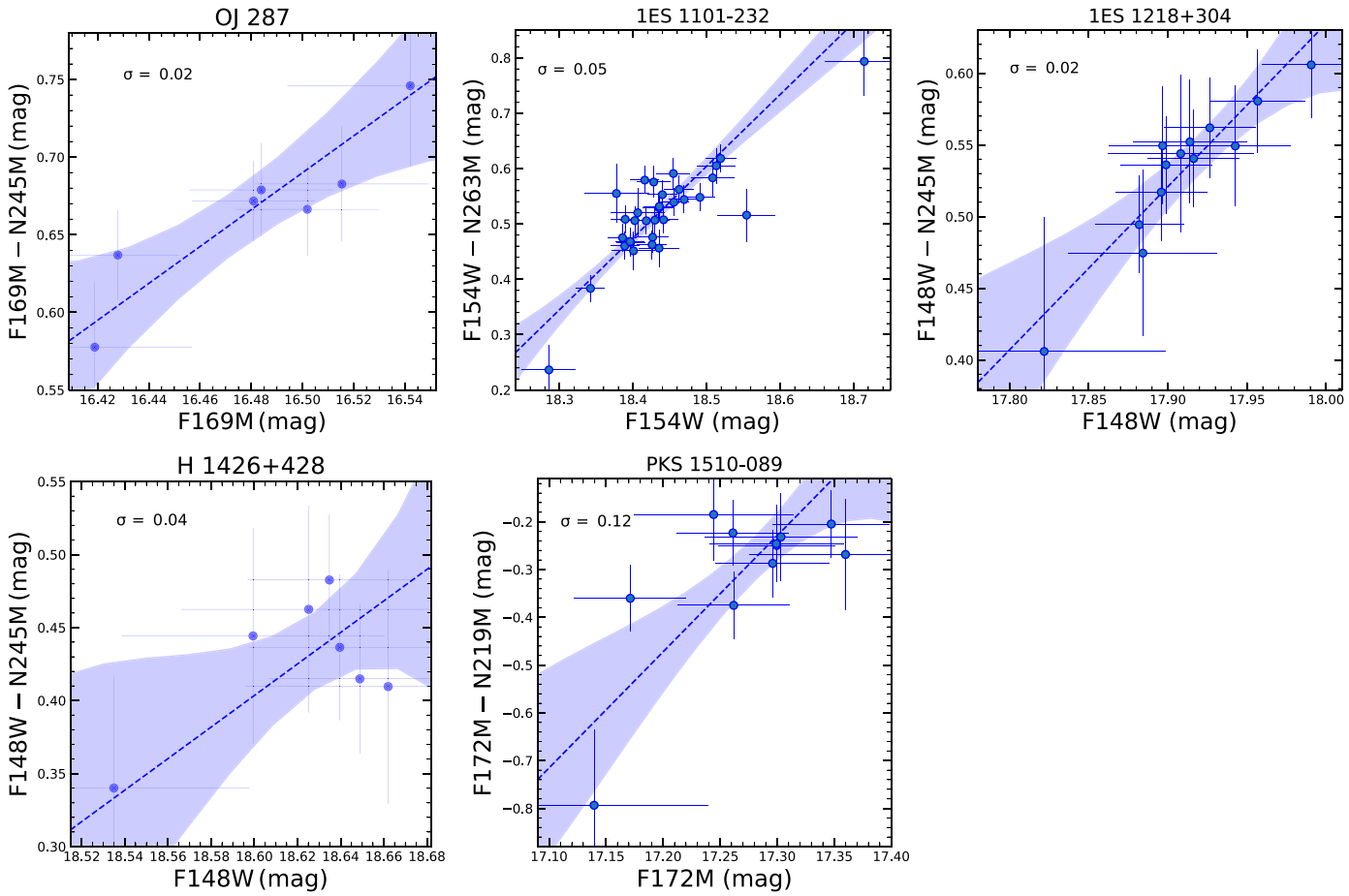

Figure 5. CMDs for the sources that are variable and have more than four simultaneous FUV and NUV photometric data points. The best-fit line from Bayesian analysis using LINMIX _ ERR is shown by the dashed blue line, and the uncertainty range on the best fit is shown by the blue shaded region. The intrinsic scatter (σ) is given in the respective plots. The names of the sources are given on the top of each panel (see also Tables 5 and 6).

Table 5
Results of Unweighted Linear Least-squares Fit to the CMD

Name	OBSID	No. of Orbits	Color/Mag	Slope	Intercept	R	P
OJ 287	T01-163T01-9000001152	07	(F169M−N245M)/F169M	1.04 ± 0.20	-16.53 ± 3.34	0.92	0.00
1ES 1101−232	G06-086T02-9000000936	32	(F154W−N263M)/F154W	1.01 ± 0.12	-18.13 ± 2.20	0.84	0.00
1ES 1218+304	G05-211T01-9000000464	13	(F148W−N245M)/F148W	1.16 ± 0.14	-20.23 ± 2.46	0.93	0.00
H 1426+428	A04-094T01-9000001942	07	(F148W−N245M)/F148W	0.66 ± 0.38	-11.79 ± 7.16	0.61	0.15
PKS 1510−089	A04-101T01-9000001984	11	(F172M−N219M)/F172M	1.85 ± 0.58	-32.19 ± 10.03	0.73	0.01

Note. Here, Column (1) gives the name of the sources, Column (2) gives the OBSID, Column (3) gives the number of orbits used in the analysis, Column (4) gives the FUV and NUV filters used to get the color and brightness, Column (5) gives the slope and the associated error, Column (6) gives the intercept and the associated error, Column (7) gives the linear correlation coefficient (R), and Column 8 gives the probability of no correlation (P). The entries with 0 in P (Column (6)) indicate that the values are less than 1×10^{-2}.

5. Discussion and Conclusions

Flux variability in blazars in UV is found to be extremely useful for getting insights into the inner region close to the SMBH, radiation mechanisms taking place in the vicinity of SMBH, and the relativistic jets. However, because intranight observations using space-based UV telescopes are time expensive, the nature of UV variability in blazars is not well studied in the literature. Recently, several studies have been conducted on large samples of optically selected quasars using their UV data obtained with GALEX (B. Punsly et al. 2016, 2021) and covering a day or longer timescales. Here, the first study was performed to explore the properties of blazars in UV on the shorter hour-like timescales. For this purpose, we concentrated on a sample of 10 blazars, comprising of two FSRQs and eight BL Lacs objects that were observed using UVIT payload on board AstroSat.

In blazars, the UV emission obtained by the instrument is widely believed to be nonthermal synchrotron emission along the jet axis. Doppler factor δ is defined as $\delta = 1/\Gamma(1 - \beta \cos\theta_{\rm obs})$, where Γ is the bulk Lorentz factor, β is the speed of emission region in the units of speed of light, and $\theta_{\rm obs}$ is the angle of the jet with respect to the line of sight to the observer. In blazars, the observer's line of sight is closely

Table 6
Results of Fit to the Points in the CMD Using BCES and Bayesian Methods

Name	OBSID	No. of Orbits	Color/Mag	BCES		Bayesian	
				Slope	Intercept	Slope	Intercept
OJ 287	T01-163T01-9000001152	07	(F169M−N245M)/F169M	1.08 ± 0.18	-17.18 ± 3.01	1.15 ± 1.02	-18.31 ± 16.74
1ES 1101−232	G06-086T02-9000000936	32	(F154W−N263M)/F154W	1.08 ± 0.17	-19.31 ± 3.19	1.29 ± 0.18	-23.35 ± 3.37
1ES 1218+304	G05-211T01-9000000464	13	(F148W−N245M)/F148W	1.04 ± 0.11	-18.14 ± 2.06	1.14 ± 0.54	-19.84 ± 9.70
H 1426+428	A04-094T01-9000001942	07	(F148W−N245M)/F148W	0.60 ± 0.32	-10.78 ± 5.97	1.07 ± 2.08	-19.50 ± 38.80
PKS 1510−089	A04-101T01-9000001984	11	(F172M−N219M)/F172M	2.75 ± 0.67	-47.89 ± 11.66	2.43 ± 1.74	-42.29 ± 30.10

Note. The columns have the same meaning as in Table 5.

aligned with the orientation of the relativist jet (C. M. Urry & P. Padovani 1995), and thus, the jet emission undergoes Doppler boosting owing to a higher apparent Lorentz factor and the jet emission overpowers the thermal radiation from the accretion disk. This is followed by a series of effects, such as amplified flux and blueshifted emitted frequencies, which causes the shortening of their apparent variability timescales (C. M. Urry & P. Padovani 1995). Because of the above reasons, blazar variability is an excellent tool for shedding light on the structure of jets and understanding the emission mechanisms taking place in them.

Various theoretical models used to explain blazar variability are broadly divided into extrinsic and intrinsic mechanisms. The probable intrinsic mechanisms include shocks traveling down the jet or magnetic irregularities or accretion-disk instabilities (R. D. Blandford & A. Königl 1979; A. P. Marscher et al. 2008; P. Mohan & A. Mangalam 2015, and references therein), whereas the extrinsic effects involve interstellar scintillation as well as variations in the viewing angle, leading to changes in the Doppler factor or gravitational microlensing (P. Schneider & A. Weiss 1987, and references therein). During the low state in blazars, UV variability can be attributed to the instabilities or hot spots on the accretion disk (S. K. Chakrabarti & P. J. Wiita 1993). However, various multiwavelength studies of these sources have demonstrated that the electromagnetic emission from all these blazars is jet dominated (A. Barnacka et al. 2014; N. Sahakyan 2020; R. Prince et al. 2021a, 2021b; P. Kushwaha et al. 2022; R. Diwan et al. 2023; P. Goswami et al. 2024). Therefore, it is tempting to postulate that the observed variable UV emission from them could be largely contributed by their Doppler-boosted relativistic jet. To further investigate this claim, we analyzed the color–magnitude relationship of the sample sources.

Blazars, a subclass of AGN, exhibit intriguing color or spectral index variations that play a crucial role in unraveling their underlying emission mechanisms. These enigmatic cosmic objects exhibit various behaviors in their CMDs. CMDs of blazars have shown to exhibit three distinct trends, namely, RWB, BWB and achromatic behaviors. Generally, most studies indicate that BWB chromatism is the dominant behavior in most of the BL Lac objects, while RWB chromatism is typical of FSRQs (F. Vagnetti et al. 2003; A. Agarwal et al. 2022, 2023, and references therein). However, the color–magnitude correlation in blazars still remains a topic of debate in literature. The BWB trend is often explained by a single-component synchrotron model where an influx of freshly injected electrons with a harder energy distribution than the previous cooler electrons leads to increased flux and a bluer spectrum. Also, electrons accelerated at the shock front have higher energies and gradually loose energy due to radiative cooling, thereby showing more variations at the higher-energy band (J. G. Kirk et al. 1998; A. Mastichiadis & J. G. Kirk 2002). The existence of an energy-stratified jet also finds support from the energy-dependent polarization observed recently in HSP blazars such as Mrk 421 (D. E. Kim et al. 2024) and 1ES 0229 +200 (S. R. Ehlert et al. 2023). Furthermore, this trend can also be elucidated by a two-component emission model. In this scenario, a stable component with a constant spectral index ($\alpha_{\rm constant}$) coexists with a variable component characterized by a flatter slope (α_1). As the variable component outshines the stable one, chromatic behaviors emerge, influencing short-term behavior (dominated by pronounced chromatic components) and longer-term variations (attributed to a mildly chromatic component). In all the sources studied for spectral variations, a BWB behavior was found, also suggesting that the variable flux seen in the sample sources could be attributed to synchrotron emission from the jet, potentially signaling an enhancement in particle acceleration efficiency. One of the FSRQs, namely PKS 1510−089, also displayed the BWB trend, thus suggesting that the jets of BL Lacs and FSRQs could be fundamentally the same.

Detailed spectral measurements of a handful of blazar jets based on examination of flux densities of the knots in the kiloparsec-scale jets hint toward the fact that a significant portion of their synchrotron UV radiation might come from relativistic particles different from those responsible for optical/IR emission. The study displays an increase toward the UV and a smooth transition to X-ray data points, thus revealing a clear spectral upturn in the optical/UV region of their SEDs (Y. Uchiyama et al. 2006). The presence of high polarization in the UV emission, as found by M. Cara et al. (2013), supports the origin of this high-energy component. The above findings have also been confirmed by K. Chand et al. (2022), who studied the optical and UV emissions (rest frame) from blazars.

The scarcity of information on the UV variability in blazars is due to the expensive nature of carrying out intranight monitoring campaigns using space-based UV telescopes (K. L. Smith et al. 2018). To tackle this challenge, recent efforts have leveraged UV data collected by GALEX for large samples of AGN. However, these studies mainly focused on day-long or longer-timescale monitoring of the optically selected quasars (B. Punsly et al. 2016), thereby examining the accretion disk rather than the relativistic jet of these sources. To delve into the rapid UV variability of blazars, UV flux variability characteristics on hourly timescales of ten blazars observed using UVIT on board AstroSat in FUV and NUV filters were studied. UV flux variations on timescales of hours was found in nine blazars. Also, the color–magnitude relationship was analyzed for the sample of sources that are found to be variable and having more than four simultaneous observations in FUV and NUV filters, namely, OJ 287, 1ES 1101−232, 1ES 1218+304, H 1426+428, and PKS 1510-089. Of these, the first four sources belong to the BL Lac category, while PKS 1510−089 is an FSRQ. Thus, both FSRQs and BL Lacs in the sample were found to display a dominant BWB chromatism in the UV region. The above findings indicate the dominance of the synchrotron emission from the Doppler-boosted jet for this sample of blazars in the UV band.

Acknowledgments

The authors extend their sincere gratitude to the anonymous reviewer for the useful comments and suggestions on the paper. This research made use of Photutils, an Astropy package for detection and photometry of astronomical sources (L. Bradley et al. 2023). This publication uses the data from the AstroSat mission of the Indian Space Research Organization (ISRO), archived at the Indian Space Science Data Centre (ISSDC). This publication uses UVIT data processed by the Payload Operations Center at the Indian Institute of Astrophysics (IIA), Bangalore. The UVIT is built in collaboration between IIA, Inter University Center for Astronomy and Astrophysics (IUCAA), Tata Institute of Fundamental Research (TIFR), ISRO and Canadian Space Agency (CSA). One of the authors (S.B.G.) thanks the IUCAA, Pune, India for the Visiting Associateship.

Appendix

In this appendix we provide the brightness measurements of all the blazars studied in this work. They are provided in a machine-readable table. Table 7 provides this data for PKS 0208−512 as an example regarding its form and content.

Table 7
Brightness Measurements of the Source PKS 0208−512

Date (dd-mm-yyyy)	Filter	MJDstart	MJDend	Mag
30-10-2016	F148W	57690.991247	57690.998305	18.28 ± 0.05
		57691.063816	57691.067698	18.37 ± 0.07
		57691.249972	57691.253182	18.42 ± 0.08
		57691.385321	57691.386868	18.50 ± 0.12
	F169M	57691.588337	57691.600612	18.22 ± 0.05
		57691.723686	57691.731484	18.25 ± 0.07
	N219M	57690.991175	57690.998355	17.31 ± 0.07
		57691.063744	57691.067748	17.39 ± 0.09
		57691.249923	57691.253181	17.38 ± 0.10
		57691.317597	57691.324360	17.44 ± 0.07
		57691.385272	57691.386868	17.33 ± 0.14
		57691.520614	57691.524076	17.53 ± 0.10
	N279N	57691.588288	57691.600612	17.09 ± 0.05
		57691.655962	57691.657762	16.93 ± 0.12
		57691.723637	57691.731484	17.09 ± 0.06
		57691.791305	57691.793444	17.06 ± 0.12
		57691.862352	57691.863146	17.04 ± 0.19
25-12-2019	F148W	58841.831743	58841.833213	18.61 ± 0.13
	F154W	58841.904312	58841.905736	18.55 ± 0.15
	F169M	58841.976881	58841.985370	18.11 ± 0.06
		58842.305330	58842.311886	18.17 ± 0.07
	F172M	58842.643654	58842.654596	17.91 ± 0.09

(This table is available in its entirety in machine-readable form in the online article.)

ORCID iDs

M. Reshma https://orcid.org/0009-0009-9149-9049
Aditi Agarwal https://orcid.org/0000-0003-4682-5166
C. S. Stalin https://orcid.org/0000-0002-4998-1861
Prajwel Joseph https://orcid.org/0000-0003-1409-1903
Akanksha Dagore https://orcid.org/0009-0001-5407-3016
Amit Kumar Mandal https://orcid.org/0000-0001-9957-6349
Ashish Devaraj https://orcid.org/0000-0001-5933-058X
S. B. Gudennavar https://orcid.org/0000-0002-9019-9441

References

Abdo, A. A., Ackermann, M., Agudo, I., et al. 2010, ApJ, 716, 30
Abdo, A. A., Ackermann, M., Ajello, M., et al. 2011, ApJ, 736, 131
Abdollahi, S., Acero, F., Ackermann, M., et al. 2020, ApJS, 247, 33
Abe, H., Abe, S., Acciari, V. A., et al. 2024, A&A, 682, A114
Acciari, V. A., Aliu, E., Arlen, T., et al. 2009, ApJ, 695, 1370
Acciari, V. A., Aliu, E., Arlen, T., et al. 2011, ApJ, 738, 169
Acciari, V. A., Aliu, E., Beilicke, M., et al. 2010, ApJL, 709, L163
Ackermann, M., Ajello, M., Atwood, W. B., et al. 2015, ApJ, 810, 14
Agarwal, A. 2023, ApJ, 946, 109
Agarwal, A., Pandey, A., Özdönmez, A., et al. 2022, ApJ, 933, 42
Agarwal, A., Mihov, B., Agrawal, V., et al. 2023, ApJS, 265, 51
Agrawal, P. C. 2017, JApA, 38, 27
Agudo, I., Jorstad, S. G., Marscher, A. P., et al. 2011, ApJL, 726, L13
Aharonian, F., Akhperjanian, A., Barrio, J., et al. 2002, A&A, 384, L23
Aharonian, F., Akhperjanian, A. G., Barres de Almeida, U., et al. 2007a, A&A, 475, L9
Aharonian, F., Akhperjanian, A. G., Bazer-Bachi, A. R., et al. 2007b, A&A, 470, 475
Ai, Y. L., Yuan, W., Zhou, H. Y., et al. 2010, ApJL, 716, L31
Akritas, M. G., & Bershady, M. A. 1996, ApJ, 470, 706
Albert, J., Aliu, E., Anderhub, H., et al. 2006, ApJL, 642, L119
Andruchow, I., Romero, G. E., & Cellone, S. A. 2005, A&A, 442, 97
Angel, J. R. P., & Stockman, H. S. 1980, ARA&A, 18, 321
Antonucci, R. 1993, ARA&A, 31, 473
Bachev, R., Semkov, E., Strigachev, A., et al. 2012, MNRAS, 424, 2625
Barnacka, A., Moderski, R., Behera, B., Brun, P., & Wagner, S. 2014, A&A, 567, A113
Bhatta, G., & Webb, J. 2018, Galax, 6, 2
Blandford, R. D., & Königl, A. 1979, ApJ, 232, 34
Blandford, R. D., & Rees, M. J. 1978, PhyS, 17, 265
Bonning, E., Urry, C. M., Bailyn, C., et al. 2012, ApJ, 756, 13
Bonnoli, G., Ghisellini, G., Foschini, L., Tavecchio, F., & Ghirlanda, G. 2011, MNRAS, 410, 368
Bradley, L., Sipőcz, B., Robitaille, T., et al. 2023, astropy/photutils: 1.12.0, 1.10.0, Zenodo, doi:10.5281/zenodo.1035865
Cai, Z.-Y., Wu, X.-B., Yang, J., et al. 2022, ApJS, 260, 47
Cara, M., Perlman, E. S., Uchiyama, Y., et al. 2013, ApJ, 773, 186
Catanese, M., Akerlof, C. W., Badran, H. M., et al. 1998, ApJ, 501, 616
Chakrabarti, S. K., & Wiita, P. J. 1993, A&A, 271, 216
Chand, K., Gopal-Krishna, Omar, A., et al. 2022, MNRAS, 511, 13
Chatterjee, R., Fossati, G., Urry, C. M., et al. 2013, ApJL, 763, L11
Cologna, G., Mohamed, M., Wagner, S., et al. 2015, 34th ICRC (ICRC2015), 34, 762
Costamante, L., Ghisellini, G., Giommi, P., et al. 2001, A&A, 371, 512
Dai, X., Zhang, B., Gou, L., & Mészáros, P. 2001, AJ, 122, 2901
Devanand, P. U., Gupta, A. C., Jithesh, V., & Wiita, P. J. 2022, ApJ, 939, 80
Diwan, R., Prince, R., Agarwal, A., et al. 2023, MNRAS, 524, 4333
Djannati-Atai, A., Piron, F., Barrau, A., et al. 1999, A&A, 350, 17
Edelson, R. 1992, ApJ, 401, 516
Edwards, P. G., & Piner, B. G. 2002, ApJL, 579, L67
Ehlert, S. R., Liodakis, I., Middei, R., et al. 2023, ApJ, 959, 61
Elvis, M., Plummer, D., Schachter, J., & Fabbiano, G. 1992, ApJS, 80, 257
Falomo, R., Kotilainen, J. K., & Treves, A. 2002, ApJL, 569, L35
Falomo, R., Pesce, J. E., & Treves, A. 1993, ApJL, 411, L63
Gaur, H., Gupta, A. C., Lachowicz, P., & Wiita, P. J. 2010, ApJ, 718, 279
Gaur, H., Gupta, A. C., Wiita, P. J., Joshi, U. C., & Bai, J. M. 2012a, MNRAS, 420, 3147
Gaur, H., Gupta, A. C., Strigachev, A., et al. 2012b, MNRAS, 425, 3002
Gaur, H., Gupta, A. C., Bachev, R., et al. 2019, MNRAS, 484, 5633
Ghisellini, G., Tavecchio, F., Foschini, L., & Ghirlanda, G. 2011, MNRAS, 414, 2674
Ghosh, S. K., Tandon, S. N., Joseph, P., et al. 2021, JApA, 42, 29
Ghosh, S. K., Tandon, S. N., Singh, S. K., et al. 2022, JApA, 43, 77
Giommi, P., Perri, M., & Fiore, F. 2000, MNRAS, 317, 743
Giroletti, M., Giovannini, G., Taylor, G. B., & Falomo, R. 2004, ApJ, 613, 752
Gliozzi, M., Sambruna, R. M., Jung, I., et al. 2006, ApJ, 646, 61
Gopal-Krishna, G. A., Joshi, S., et al. 2011, MNRAS, 416, 101
Goswami, P., Zacharias, M., Zech, A., et al. 2024, A&A, 682, A134
Grube, J. 2008, American Institute of Physics Conference Series, Vol. 1085 (AIP), 662
Gu, M., Lee, C.-U., Pak, S., Yim, H., & Fletcher, A. 2006, A&A, 450, 39
H. E. S. S. Collaboration, Abramowski, A., Acero, F., et al. 2013, A&A, 554, A107
Hartman, R. C., Bertsch, D. L., Bloom, S. D., et al. 1999, ApJS, 123, 79
Healey, S. E., Romani, R. W., Cotter, G., et al. 2008, ApJS, 175, 97
Horan, D., Badran, H. M., Bond, I. H., et al. 2002, ApJ, 571, 753
Hovatta, T., Lindfors, E., Blinov, D., et al. 2016, A&A, 596, A78
Huang, S., Hu, S., Yin, H., et al. 2022, MNRAS, 515, 2778
Jannuzi, B. T., Smith, P. S., & Elston, R. 1994, ApJ, 428, 130
Joseph, P., Stalin, C. S., Tandon, S. N., & Ghosh, S. K. 2021, JApA, 42, 25
Kelly, B. C. 2007, ApJ, 665, 1489
Kim, D. E., Di Gesu, L., Liodakis, I., et al. 2024, A&A, 681, A12
Kirk, J. G., Rieger, F. M., & Mastichiadis, A. 1998, A&A, 333, 452
Kushwaha, P., Singh, K. P., Sinha, A., et al. 2022, ICRC (Berlin), 37, 644
Lachowicz, P., Gupta, A. C., Gaur, H., & Wiita, P. J. 2009, A&A, 506, L17
Li, H.-Z., Guo, D.-F., Qin, L.-H., et al. 2024, MNRAS, 528, 6823
Lynden-Bell, D. 1969, Natur, 223, 690
MAGIC Collaboration, Acciari, V. A., Ansoldi, S., et al. 2018, A&A, 619, A159

MAGIC Collaboration, Acciari, V. A., Ansoldi, S., Antonelli, L. A., et al. 2020, MNRAS, 496, 3912
Marscher, A. P., Jorstad, S. G., D'Arcangelo, F. D., et al. 2008, Natur, 452, 966
Marshall, H. L., Urry, C. M., Sambruna, R. M., & Pesce, J. E. 2001, ApJ, 549, 938
Mastichiadis, A., & Kirk, J. G. 2002, PASA, 19, 138
Mohan, P., & Mangalam, A. 2015, ApJ, 805, 91
Moo, K. E., Bregman, J. N., & Reynolds, M. T. 2022, ApJ, 931, 83
Negi, V., Joshi, R., Chand, K., et al. 2022, MNRAS, 510, 1791
Nolan, P. L., Abdo, A. A., Ackermann, M., et al. 2012, ApJS, 199, 31
Obrien, P. T., Gondhalekar, P. M., & Wilson, R. 1988, MNRAS, 233, 845
O'Dell, S. L., Puschell, J. J., Stein, W. A., & Warner, J. W. 1978, ApJS, 38, 267
Otero-Santos, J., Acosta-Pulido, J. A., Becerra González, J., et al. 2022, MNRAS, 511, 5611
Paliya, V. S., Marcotulli, L., Ajello, M., et al. 2017, ApJ, 851, 33
Paliya, V. S., Parker, M. L., Fabian, A. C., & Stalin, C. S. 2016, ApJ, 825, 74
Paliya, V. S., Sahayanathan, S., & Stalin, C. S. 2015, ApJ, 803, 15
Pandey, A., Gupta, A. C., Damljanovic, G., et al. 2020, MNRAS, 496, 1430
Pandey, A., Gupta, A. C., & Wiita, P. J. 2017, ApJ, 841, 123
Pandey, A., Gupta, A. C., & Wiita, P. J. 2018, ApJ, 859, 49
Pandey, A., Rajput, B., & Stalin, C. S. 2022, MNRAS, 510, 1809
Pandey, S. B., Gupta, A. C., Wiita, P. J., et al. 2020, MNRAS, 496, 1430
Peceur, N. W., Taylor, A. R., & Kraan-Korteweg, R. C. 2020, MNRAS, 495, 2162
Perlman, E. S., Stocke, J. T., Schachter, J. F., et al. 1996, ApJS, 104, 251
Pian, E., Vacanti, G., Tagliaferri, G., et al. 1998, ApJL, 492, L17
Piner, B. G., Pant, N., & Edwards, P. G. 2008, ApJ, 678, 64
Prince, R., Agarwal, A., Gupta, N., et al. 2021, A&A, 654, A38
Prince, R., Agarwal, A., Gupta, N., et al. 2021a, A&A, 654, A38
Prince, R., Raman, G., Khatoon, R., et al. 2021b, MNRAS, 508, 315
Punsly, B., Frey, S., Reynolds, C., et al. 2021, ApJ, 919, 40
Punsly, B., Marziani, P., Zhang, S., Muzahid, S., & O'Dea, C. P. 2016, ApJ, 830, 104
Raiteri, C. M., Villata, M., Acosta-Pulido, J. A., et al. 2017, Natur, 552, 374
Rajput, B., Pandey, A., Stalin, C. S., & Mathew, B. 2022, MNRAS, 517, 3236
Rajput, B., Shah, Z., Stalin, C. S., Sahayanathan, S., & Rakshit, S. 2021, MNRAS, 504, 1772
Rajput, B., Stalin, C. S., & Sahayanathan, S. 2020, MNRAS, 498, 5128
Rakshit, S. 2020, A&A, 642, A59
Rakshit, S., Stalin, C. S., Muneer, S., Neha, S., & Paliya, V. S. 2017, ApJ, 835, 275
Ramakrishnan, V., Hovatta, T., Tornikoski, M., et al. 2016, MNRAS, 456, 171
Rees, M. J. 1984, ARA&A, 22, 471
Ren, H. X., Cerruti, M., & Sahakyan, N. 2023, A&A, 672, A86
Rieger, F. M., & Volpe, F. 2010, A&A, 520, A23
Romero, G. E., Cellone, S. A., & Combi, J. A. 1999, A&AS, 135, 477
Romero, G. E., Cellone, S. A., Combi, J. A., & Andruchow, I. 2002, A&A, 390, 431
Roy, A., Sarkar, A., Chatterjee, A., et al. 2022, MNRAS, 510, 3641
Sahakyan, N. 2020, MNRAS, 496, 5518
Saito, S., Stawarz, Ł., Tanaka, Y. T., et al. 2013, ApJL, 766, L11
Sandrinelli, A., Covino, S., & Treves, A. 2014, ApJL, 793, L1
Schneider, P., & Weiss, A. 1987, A&A, 171, 49
Sillanpaa, A., Haarala, S., Valtonen, M. J., Sundelius, B., & Byrd, G. G. 1988, ApJ, 325, 628
Smith, K. L., Mushotzky, R. F., Boyd, P. T., et al. 2018, ApJ, 857, 141
Stalin, C. S., Kawabata, K., Uemura, M., et al. 2009, MNRAS, 399, 1357
Sukanya, N., Stalin, C. S., Joseph, P., et al. 2018, JApA, 39, 65
Tandon, S. N., Ghosh, S. K., Hutchings, J., Stalin, C. S., & Subramaniam, A. 2017, CSci, 113, 583
Tandon, S. N., Postma, J., Joseph, P., et al. 2020, AJ, 159, 158
Thompson, D. J., Djorgovski, S., & de Carvalho, R. 1990, PASP, 102, 1235
Uchiyama, Y., Urry, C. M., Cheung, C. C., et al. 2006, ApJ, 648, 910
Ulrich, M.-H., Maraschi, L., & Urry, C. M. 1997, ARA&A, 35, 445
Urry, C. M., & Mushotzky, R. F. 1982, ApJ, 253, 38
Urry, C. M., & Padovani, P. 1995, PASP, 107, 803
Urry, C. M., Maraschi, L., Edelson, R., et al. 1993, ApJ, 411, 614
Vagnetti, F., Trevese, D., & Nesci, R. 2003, ApJ, 590, 123
Veron-Cetty, M.-P., & Veron, P. 2010, A&A, 518, A10
Villata, M., Raiteri, C. M., Kurtanidze, O. M., et al. 2002, A&A, 390, 407
Villata, M., Raiteri, C. M., Kurtanidze, O. M., et al. 2004, A&A, 421, 103
Wagner, S. J., & Witzel, A. 1995, ARA&A, 33, 163
Webb, J. R. 2021, Galax, 9, 69
Welsh, B. Y., Wheatley, J. M., & Neil, J. D. 2011, A&A, 527, A15
Yuan, Q., Kushwaha, P., Gupta, A. C., et al. 2023, ApJ, 953, 47
Zeng, W., Hu, W., Zhang, G.-M., et al. 2019, PASP, 131, 074102
Zhang, Z., Gupta, A. C., Gaur, H., et al. 2021, ApJ, 909, 103